

High Pressure Structural Stability of Multiferroic Hexagonal $REMnO_3$

P. Gao¹, Z. Chen¹, T. A. Tyson^{1,2}, T. Wu¹, K. H. Ahn^{1,2}, Z. Liu³, R. Tappero⁴
S. B. Kim² and S.-W. Cheong²

¹Department of Physics, New Jersey Institute of Technology, Newark, NJ 07102

²Rutgers Center for Emergent Materials and Department of Physics & Astronomy,
Rutgers University, Piscataway, NJ 08854

³Geophysical Laboratory, Carnegie Institution of Washington, DC 20015

⁴National Synchrotron Light Source, Brookhaven National Laboratory, Upton, NY, USA

Abstract

Structural changes in $REMnO_3$ ($RE= Y, Ho, Lu$) under high pressure were examined by synchrotron x-ray diffraction methods at room temperature. Compression occurs more readily in the ab plane than along the c -axis. Under hydrostatic pressure (~ 11 GPa), the atoms hold their approximate ambient fractional positions in the unit cell and the spontaneous polarization shows no significant change. With increased pressure, a pressure-induced hexagonal to orthorhombic phase transition was observed starting at ~ 22 GPa for $Lu(Y)MnO_3$. A small volume fraction of $Lu(Y)MnO_3$ is converted to the orthorhombic phase when the pressure is increased to 35 GPa and the orthorhombic phase is maintained on pressure release. High pressure IR absorption spectroscopy and Mn K-edge near edge x-ray absorption spectroscopy confirm that the hexagonal $P6_3cm$ structure is stable below ~ 20 GPa and the environment around Mn ion is not changed. Shifts in the unoccupied p -band density of states with pressure are observed in the Mn K-Edge spectra. A schematic pressure-temperature phase diagram is given for the small ion $REMnO_3$ system.

PACS: 62.50.-p, 61.05.cp, 78.30.Hv, 61.05.cj, 64.30.Jk

I. Introduction

The rare-earth (*RE*) manganites (such as $RE\text{MnO}_3$, $RE\text{Mn}_2\text{O}_5$ and $RE_2\text{Mn}_2\text{O}_7$) are a group of systems with interesting properties which have attracted interest from the fundamental and basic physics perspectives [1]. The $RE\text{MnO}_3$ systems fall into two basic structures: hexagonal and orthorhombic phase depending on the ionic radius of r . Small ionic radius $RE\text{MnO}_3$ systems ($RE = \text{Ho-Lu, Y}$) are in the hexagonal structure and exhibits both ferroelectric and magnetic properties. The magnetic ordering temperature T_N is ~ 90 K [2] and the ferroelectric ordering temperature T_C is near ~ 900 K. The low-high temperature phase transition is predicted to pass through several aristotype phases [3]. The hexagonal structure ($P6_3cm$, $Z = 6$) is built up of MnO_5 trigonal bipyramids, which are illustrated in Fig. 1. In the basal (ab) plane, the pyramids are linked at the base corners to construct a triangular lattice. The *RE* ions are located between these MnO_5 layers and are linked with oxygen atoms. Each consecutive (ab plane) layer of MnO_3 (Fig. 1(b)) is rotated by 180° about the c -axis. They are geometrically frustrated antiferromagnetic materials [4]. The Mn^{3+} spins and the associated magnetic exchange are confined to the basal (ab) plane, and Mn^{3+} magnetic ground state produces a 120° angle between spins on local Mn triangles.

A first order structural transition occurs near 1200 K on cooling from the high temperature centrosymmetric $P6_3mmc$ ($Z=2$) phase to an asymmetric low temperature $P6_3cm$ phase. The onset of the ferroelectricity with the spontaneous polarization \mathbf{P}_s along c -axis [5] is observed to occur near $T_C \sim 900$ K. If the high temperature is accompanied with the high pressure (~ 4 GPa and ~ 1000 °C) [6, 7, 8], the hexagonal (Hex) compound will be converted into a corresponding orthorhombic (Ortho) phase, which has a higher density and is strongly Jahn-Teller distorted [9]. By other techniques such as chemical solution method [10] and epitaxial thin film growth techniques [11,12], the orthorhombic compound also can be made. On an appropriate perovskite substrate, the hexagonal $RE\text{MnO}_3$ is forced into the orthorhombic form [11]. In other words, substrate strain can stabilize the orthorhombic phase for small ion sizes. Vice versa, the substrate like ZrO_2 (Y_2O_3) (YSZ) can epitaxially stabilize Hex- DyMnO_3 and Hex- TbMnO_3 films, which are normally in the orthorhombic structure [12]. When the normal Hex- $RE\text{MnO}_3$ films are deposited on the YSZ substrate, the lattice parameter c of the film in the out-of-plane direction is tuned by the film

thicknesses [12]. If the cell is elongated along c -axis, it would enhance the spontaneous polarization value. In a relaxed Hex- $REMnO_3$ film, the T_N value is lower than the value of the bulk material [13].

Under high pressure conditions, the dielectric and magnetic properties of Hex- $REMnO_3$ have been studied [14, 15, 16, 17, 18] up to 6 GPa. In those works, the hexagonal structure is not changed [15, 19]. The spin rotation transition temperature (T_{SR}) decreases linearly with applied pressure at a rate of $dT_{SR}/dp = -2.05$ K/GPa [14]. The Mn magnetic moment is suppressed. At 10 K, the ordered magnetic moment values are reduced with rates $dM/dP = -0.35$ μ_B GPa $^{-1}$ in $YMnO_3$ and -0.08 μ_B/Mn GPa $^{-1}$ in $LuMnO_3$ [16, 17]. The decrease in $LuMnO_3$ is due to an enhancement of the geometrical frustration effects on the triangular lattice. At the same time, the magnetic symmetry of the triangular AF state (the irreducible representation Γ_2) remains unchanged. However, spin reorientation of Mn magnetic moments and a change in the symmetry of the AF structure occur in $YMnO_3$. A spin-liquid state due to magnetic frustration on the triangular lattice forms by Mn ions at normal pressure and $T > T_N = 70$ K, and an ordered triangular AF state occurs with the symmetry of the irreducible representation Γ_1 arises at $T < T_N$. The high-pressure effect leads to a spin reorientation of Mn magnetic moments and a change in the symmetry of the AF structure, which can be described by a combination of the irreducible representations Γ_1 and Γ_2 [16, 17, 18]. High pressure induces a spin-liquid phase in $YMnO_3$, coexisting with the suppressed long-range AF order. The spin liquid phase exhibits a temperature dependence distinctively different from short-range spin correlations seen at ambient pressure. Its formation occurs through an in-plane Mn-O bond symmetrization and results in reduced magnetoelastic coupling at high pressures [19].

Structurally, high pressure Raman spectroscopy reveals the possibility of a hexagonal-orthorhombic phase transition happening at room temperature induced by pressure [20]. In a Hex- $Ho_{0.8}Dy_{0.2}MnO_3$, the phase transition pressure is interpreted to occur at ~ 10 GPa by observation of new phonons. No combined systematic study of the structure of Hex- $REMnO_3$ under pressure has been conducted on this system to date.

In this work, present the hydrostatic and quasi-hydrostatic pressure effects on $REMnO_3$ ($R = Y, Ho, Lu$) to explore how the structural, vibrational and optical properties change with pressure. To effect this, synchrotron based x-ray diffraction (XRD), x-ray spectroscopy (XAS) and infrared (IR) methods are utilized at room temperature (298 K). We find that a pressure-induced a hexagonal-orthorhombic phase

transition requires a high pressure (~ 22 GPa) for Lu(Y)MnO₃ and results in only small fractional conversion of Lu(Y)MnO₃ to the orthorhombic phase at room temperature. The hexagonal *REMnO₃* is very stable below ~ 20 GPa. Under hydrostatic pressure (~ 11 GPa), the atoms hold their fractional positions. By checking the dipole moment in a unit cell, we find that the spontaneous polarization is a constant value under hydrostatic pressures up to ~ 11 GPa. The x-ray near edge absorption spectrum and IR absorption spectrum confirm that *P6₃cm* is a stable structure under ~ 20 GPa and the environment around the Mn ion is not changed. These results imply that the high temperature conversion to the orthorhombic is strongly kinetically driven.

II. Experimental and Computational Methods

Finely grinded *REMnO₃* polycrystalline powders made by the solid-state reaction method were sealed into a diamond anvil cell (DAC) with three to four ruby chips for pressure calibration. Monochromatic X-ray ($\lambda = 0.4066$ Å) powder diffraction under high pressures was completed at the X17C beam line at the National Synchrotron Light Source (NSLS), in Brookhaven National Laboratory. A charge-coupled device (Mar, 2048×2048 pixels with 80 μm resolution) was used to record the 2-D diffraction rings. The integration of the data to yield intensity vs. 2θ diagrams was conducted by the program Fit2D [21]. Methanol/Ethanol/Water (16:3:1) mixture was used as the pressure medium in x-ray diffraction experiments, whose glass transition pressure is ~ 10.5 GPa [22]. The pressure dependent synchrotron infrared (IR) absorption spectra were measured at the U2A beam line, at NSLS. A vacuum infrared microscope provided resolution of 4 cm^{-1} in far IR ($100 - 650$ cm^{-1}) range. It was equipped with a 3.5 -micron Mylar beam splitter, a 40 mm working distant reflecting objective and a Si bolometer detector. CsI was used to dilute the *REMnO₃* powder and acted as the pressure medium in IR absorption measurements. The pressures generated by DAC were calibrated by the Ruby Fluorescence method. The transmission mode x-ray absorption measurements were performed at beamline X27A at the Mn K-Edge in a DAC utilizing a pair of partially perforated diamond anvils. The pressure calibration was based on the

compression curves [23, 24] from the Fe XAFS spectra of a thin Fe metal layer loaded in the cell with the sample.

To determine the nature of the fastest varying IR modes, the eigenvectors and eigenvalues of the dynamic matrix were calculated following the approach taken previously in HoMnO₃ [25]. The structure as function of pressure was simulated in the density functional calculations using the projector augmented wave approach [26] for YMnO₃ and LuMnO₃ (with no open *RE* *f*-shells).

III. Results and Discussion

Diffraction patterns of *REMnO₃* are shown in Fig. 2(a) for the pressure range up to ~17 GPa. At ambient pressure, three hexagonal phases show similar diffraction patterns. The lattice parameters (*a* and *c*) are *a* = 6.11505 Å, *c* = 11.3781 Å (YMnO₃); *a* = 6.13450 Å, *c* = 11.41790 Å (HoMnO₃); and *a* = 6.04845 Å, *c* = 11.38300 Å (LuMnO₃) at ambient pressure, were extracted by the Rietveld method [27]. These values agree with the published results [7] (YMnO₃ *a* = 6.14666 Å, *c* = 11.4411 Å, HoMnO₃ *a* = 6.13820 Å, *c* = 11.4118 Å and LuMnO₃ *a* = 6.03011 Å, *c* = 11.3648 Å). When the crystal cell is squeezed, the diffraction peaks shift toward high *2θ* value and the peak intensities are varied as expected. However, it is a continuous process and no new peak appearing in this pressure range (up to 17 GPa). Pressure

$$V(P) = V_0 \left(1 + B_0' \frac{P}{B_0}\right)^{-1/B_0'}$$

dependence of the volume was fit by the Murnaghan equation of state:

where *V*₀, *B*₀ and *B*₀' are the volume for a solid, the zero pressure bulk modulus and the bulk modulus pressure derivative. For the typical ortho-LaMnO₃, the values of *B*₀ and *B*₀' are 108 ± 2 GPa, 8.5 ± 0.4 [28]. For the hexagonal phase, the *B*₀ values are 112±8 GPa (YMnO₃), 130±7 GPa (HoMnO₃) and 109±12 GPa (LuMnO₃). A highly anisotropic compressibility of *P6₃cm* structure is indicated by the *B*₀' values 12, 14 and 26 respectively, comparing to the *Pbnm* orthorhombic structure. The pressure dependent variation of *a* is about twice as the change for *c*. In the *ab* plane, the cell is much easier to be compressed than along *c* direction. Fig. 2(b) and (c) illustrate the pressure dependent cell volume change and lattice *a*, *c* variations. By DFT method, the volume and structural parameters of YMnO₃ and LuMnO₃ are calculated. DFT results show a coincidence with the experimental result on the pressure dependent cell volume

change. While the YMnO_3 system is well matched by the model, the LuMnO_3 with a closed $4f$ shell is not well modeled.

At ambient condition, Mn is approximately in the centre of its oxygen environment [29]. The x-ray scattering factor of oxygen is small compared to RE and Mn and hence will have higher uncertainties for the O atomic positions. By neutron diffraction, the structure under pressure has been determined up to 6 GPa [16, 17]. Here it is found that the oxygen position parameters do not vary with pressure. Moreover, in the DFT simulations the same trend is observed up to 10 GPa. Hence in our fit process, the oxygen atoms are fixed and only the heavy metallic atomic positions (RE and Mn) are adjusted. Below 11 GPa, the structure fit shows that the atomic positions of Mn and RE hold the original positions: $RE1$ at $2a$ (0, 0, $\sim 1/4$) and $RE2$ at $4b$ ($1/3, 2/3, \sim 1/4$), Mn at $6c$ ($\sim 1/3, 0, \sim 0$), which is plotted in Fig. 3(a). Beyond 11 GPa, an accurate Rietveld fit is not feasible due to distortion of the peak shapes by the glass transition of the pressure medium (non-hydrostatic conditions). However, the diffraction peak positions which determine the lattice parameters remain stable. By comparing the distances (below 11 GPa) between the Lu and Mn ions (Mn-Lu1 and Mn-Lu2 distances) in Fig. 3(b), we found that those values are conserved. This implies that the heavy atoms framework is unchanged (and the buckling of the layers is maintained at least up to 11 GPa); the oxygen atoms will be embedded into this framework as under normal pressure conditions.

To verify those results, the pressure dependent near edge x-ray absorption spectrum measurement on LuMnO_3 and IR optical density (OD) spectrum measurements on all three samples were conducted. The Mn K-edge near edge x-ray absorption spectrum of Hex- LuMnO_3 was measured as a function of pressure up to 16 GPa in a diamond anvil pressure cell, which is shown in Fig. 4. No changes in the overall shape of profile were observed indicating no significant change in the space group up to this pressure. However, an expected shift in the main features is observed (the main “ $1s$ to $4p$ ” peak move up by ~ 1.5 eV with between ambient and 16 GPa pressure). The shift in the peak position is predicted by the “Natoli Rule” [30] given by $(E_r - E_b)r^2 = \text{constant}$, where E_r is the resonance position ($4p$ here) and E_b is a reference bound state position (pre-edge here). Compression of a coordination shell of radius r about Mn will shift the resonance position to higher energies. This is what is observed. The results are consistent with the Mn K-Edge measurements of Hex- ScMnO_3 [8] ($a = 5.8308 \text{ \AA}$ and $c = 11.1763 \text{ \AA}$) compared to Hex- YMnO_3 [8] (6.1483 \AA and $c = 11.4131 \text{ \AA}$) revealing a shift of the Sc system to features to higher energy compared to that for the

Y system [31]. In both cases, the gross symmetry of the structure is preserved as can be seen in the overall profile shape [30].

To explore the pressure dependence at higher pressure, the pressure dependent IR optical density (OD) spectra are displayed in Fig. 5(a), 5(b), 5(c). The pressure medium CsI has an absorption line below 100 cm^{-1} at ambient pressure and a broad transparent region in $100 - 650\text{ cm}^{-1}$. Pressure does not add any new features to the spectrum of CsI except shifting the absorption peak (the tail $\sim 100\text{ cm}^{-1}$). The Hex-*REMnO*₃ has 23 IR active phonon modes (9A₁+ 14E₁) [32]. In our work, the ambient *REMnO*₃ absorption spectrum shapes agree with the published results of *YMnO*₃ [32]. 11 Lorentzian oscillators [32] can index our ambient *YMnO*₃ OD spectrum well. When the pressure is applied, at $\sim 12\text{ GPa}$, a phonon $\sim 375\text{ cm}^{-1}$ is separated from the phonon at $\sim 351\text{ cm}^{-1}$, which is original $\sim 308\text{ cm}^{-1}$ (symmetry E₁, labeled D) at ambient pressure, and the absorption lines of 265 cm^{-1} (A₁, labeled B) and 281 cm^{-1} (E₁, labeled C) merges into one at 301 cm^{-1} at $\sim 14\text{ GPa}$. *HoMnO*₃ and *LuMnO*₃ show more than 11 IR sensitive modes in the OD spectra in Fig. 5(b) and 5(c). For the sample of *HoMnO*₃, an oscillation line near $\sim 313\text{ cm}^{-1}$ (labeled E) is clearly seen at ambient pressure. When the pressure reaches $\sim 16.5\text{ GPa}$, two phonons with energy 256 cm^{-1} (labeled B) and 268 cm^{-1} (labeled C) will merge. In Fig. 5(c) of the *LuMnO*₃ sample, vibrations with a maximum at $\sim 333\text{ cm}^{-1}$ (labeled E) and $\sim 416\text{ cm}^{-1}$ (ambient pressure, near label F) and 515 cm^{-1} ($\sim 1.74\text{ GPa}$, near label J) can be found. Near $\sim 14.6\text{ GPa}$, the ambient vibrations 268 cm^{-1} (labeled B) and 286 cm^{-1} (label C) are merging into $\sim 293\text{ cm}^{-1}$ and phonons at $\sim 503\text{ cm}^{-1}$, $\sim 515\text{ cm}^{-1}$ (near label J) are becoming one at $\sim 10.9\text{ GPa}$. The single phonon with a frequency $\sim 400\text{ cm}^{-1}$ (ambient, labeled F) turns into two phonons $\sim 432\text{ cm}^{-1}$ and $\sim 456\text{ cm}^{-1}$ at $\sim 20.5\text{ GPa}$. The pressure dependent phonon frequencies are plotted in Fig. 6. There is no abrupt profile shape change in the OD spectra. The phonon split and merger are not the indicator of a phase change, but they only show that the structure modifies under hydrostatic pressure and depends slightly on ion size and possibly ion shape (presence of *f*-electrons).

Natural *DyMnO*₃ is an orthorhombic phase and the OD spectrum is a typical example (Fig. 5 (d)). The high pressure Hex-*REMnO*₃ OD spectra are compared with *DyMnO*₃ OD spectrum. No characteristic peaks in common were found between the Hex-*REMnO*₃ OD spectrum and the Ortho-*DyMnO*₃ OD spectrum, even at the pressure $\sim 20\text{ GPa}$. Because of the structure difference of bipyramidal (*MnO*₅) and octahedral (*MnO*₆), the spectrum shapes show a big difference in the region $\sim 300-550\text{ cm}^{-1}$. In the

hydrostatic pressure condition, the phonons are hardening with pressures and the intensity redistributed. They indicate that the crystal structure is slightly modified. The OD spectra doesn't show evidences for a structural phase transition and it confirms the result of that the $P6_3cm$ is stable structure under the high pressure. That implies that in the synthesis of meta-stable orthorhombic materials, the heat treatment plays the key role in the thermal dynamic process. With the thermal treatment (the temperature ~ 1000 K), the atoms would acquire enough energy to overcome chemical barriers required to break bonds needed to construct a new distinct and symmetry under pressure (~ 4 GPa).

To explore possible temperature dependence, we look at the OD spectra at fixed pressure but varying temperatures. The Fig. 7 is the OD spectra taken for temperatures up to 673 K with pressure at ~ 10 GPa. (The temperature was kept below 800 K [33] to avoid damage the diamond cell resulting from loss of adhesive holding the diamonds to the seats). No phase change was observed to occur during the heating process. The spectra have the same peak positions and peak profiles after cooling the LuMnO_3 sample down to the room temperature. This again points to the fact that high temperature is the driving mechanism for overcoming the barrier.

We now look in detail at the phonon pressure dependence. Systematically, the phonons harden with the pressure. The phonons in LuMnO_3 and HoMnO_3 are more sensitive with the pressure than phonons in YMnO_3 . For the three samples, the phonons with a large hardening rate occur at 310 cm^{-1} (labeled D) with $2.74 \text{ cm}^{-1}/\text{GPa}$ (YMnO_3), 313 cm^{-1} (labeled E) with $3.2 \text{ cm}^{-1}/\text{GPa}$ (HoMnO_3), 305 cm^{-1} (labeled D) and 332 cm^{-1} (labeled E) with $2.3 \text{ cm}^{-1}/\text{GPa}$ and $2.9 \text{ cm}^{-1}/\text{GPa}$ (LuMnO_3). They are attributed to E1 mode [32], which is corresponding to the motions of atoms O1, O2, O3 along a positive direction and atom O4, Mn along a negative direction in the ab plane. By calculating the E1 symmetry phonon modes for LuMnO_3 near $\sim 310 \text{ cm}^{-1}$ by the density functional method, we find that the most pressure sensitive mode is mainly due to the motion of oxygen atoms. The oxygen atoms have significant oscillatory amplitudes with O ions moving in ab plane under high pressure. Fig. 8 displays the calculated displacement amplitudes and directions as vectors of O atoms of E1 near ($\sim 310 \text{ cm}^{-1}$) symmetry phonon modes in ambient pressure LuMnO_3 .

Given the atomic positions, the polarization can be calculated from the total dipole in a unit cell volume ($\vec{P} = \sum_i \vec{x}_i Q_i$). In the Hex-*REMnO*₃, the born effective charge is found to be close to the formal charge [34]. For a high temperature symmetric structure (P6/mmc), the total dipole moment is zero. For the ferroelectric P6₃cm, the dipole moment in *ab* plane is zero and the net dipole is only along the *c*-axis. The polarizations listed in Table 1 were calculated by ambient structure data with formal charge values, where the experimental polarization amplitude of Hex-YMnO₃ is 5.5 $\mu\text{C}\cdot\text{cm}^{-2}$ [35]. We estimate the polarization amplitude of Hex-LuMnO₃ sample with the lattice parameters from the structure fit, and plot it in the Fig. 9. Because the crystal structure persists under pressures and the atoms hold their fractional positions, the polarization shows an approximately constant value in the hydrostatic pressure range up to ~11 GPa.

We now explore changes at higher quasi-hydrostatic pressures (up to 35 GPa) by x-ray diffraction method again. At ~23 GPa, new peaks appear in the x-ray diffraction patterns of YMnO₃ and LuMnO₃, which can not be indexed by a hexagonal structure. Normalized high pressure diffraction patterns of LuMnO₃ and YMnO₃ are plotted in Fig. 10 (a) and (b). These new peaks could be a sign of a new phase. We attribute them to the orthorhombic phase. A simulation of the orthorhombic phase is given as the top curve in each figure. For LuMnO₃, around ~22 GPa, the new peaks appear at $2\theta = 6.8^\circ$ and 10.7° . With pressure increased to ~35 GPa, the new peak intensities continuously grow. After releasing the pressure, these peaks retain. The peaks can be the ortho-LuMnO₃ peak (111) at $2\theta = 6.76^\circ$ and the peak (022/211) at $2\theta = 11.3^\circ$. On the other hand for YMnO₃, only one new peak appears ($2\theta = 10.94^\circ$ at ~24 GPa) and is observed to increase with pressure. It is attributed to the ortho-YMnO₃ peak (022/211). Because the characteristic (002) peak of Hex-*REMnO*₃ persists at all pressures for both LuMnO₃ and YMnO₃ samples, the x-ray diffraction patterns must be from a mixture of hexagonal and orthorhombic phases. Only small amounts of Hex-*REMnO*₃ are converted into orthorhombic phase for pressures up to ~35 GPa at room temperature.

Including data points from our measurements and the literature (given below), a qualitative pressure-temperature (P-T) phase diagram of the *REMnO*₃ system (based on the classic YMnO₃) is plotted in the Fig. 11. At ambient pressure, below ~1100 K, the system is in the P6₃mc phase [3]. YMnO₃ will start to

decompose when the temperature reaches ~ 1200 K [36,37]. Based on group theory arguments, the aristotype phases will be $P6_3/mcm$ at 1105 – 1360 K, $P6_3/mmc$ at 1360 – 1600 K and $P6/mmm$ above 1600 K [3]. The lowest pressure for forming Ortho- $YMnO_3$ reported to date was ~ 3.4 GPa at ~ 920 K [38]. Based on our fixed temperature and fixed temperature experiments we deduce a mixed phase region of Hex- $YMnO_3$ and Ortho- $YMnO_3$ existing for temperatures below 920 K. When temperature is higher than 1270 K [7, 6, 39, 38], the required phase transition pressure is reduced significantly. Except the pressure and temperature, another important factor is the duration time at fixed temperature and pressure, which can not be addressed here. Holding the Hex- $YMnO_3$ at high temperature and high pressure for a long time enhances the transformation.

IV. Summary

In conclusion, we have explored the hexagonal $REMnO_3$ structure under hydrostatic and quasi-hydrostatic pressures. The hexagonal $REMnO_3$ is a very stable phase for pressures under ~ 20 GPa at ambient temperature. The unit cell is more readily compressed in the ab plane. A phase transition is initiated above ~ 22 GPa. Below ~ 11 GPa, the Mn and RE hold the fractional positions and the polarization of $REMnO_3$ does not change with the pressure. Beyond ~ 11 GPa, without thermal treatment, no significant phase change occurs in the Hex- $REMnO_3$ for pressures up to 22 GPa. The structure of hexagonal $REMnO_3$ is stable, but the atomic displacements show strong anisotropic property. O atoms are most pressure sensitive ions, which have significant oscillation amplitudes with O ions moving in ab plane. At ~ 22 GPa, the hexagonal phase is starting to be converted into the metastable orthorhombic phase, but the hexagonal phase is still the majority phase.

V. Acknowledgments

This research was funded by DOE Grant DE-FG02-07ER46402 (NJIT) and DE-FG02-07ER46382 (Rutgers). The U2A beam line at the National Synchrotron Light Source is supported by COMPRES, the Consortium for Materials Properties Research in Earth Sciences under NSF Cooperative Agreement EAR01-35554, U.S. Department of Energy (DOE-BES and NNSA/CDAC). Use of NSLS at Brookhaven National Laboratory, was supported by the U.S. Department of Energy, Office of Science, Office of Basic Energy Sciences, under Contract No. DE-AC02-98CH10886. This research used resources of the National

Energy Research Scientific Computing Center, which is supported by the Office of Science of the U.S.
DOE under Contract No. DE-AC02-05CH11231.

Table 1. The dipole moment and polarization of Y(Lu)MnO₃ in a P6₃cm unit cell (ambient pressure)*

	Dipole ($e\text{\AA}$)	Polarization ($\mu\text{C cm}^{-2}$)
YMnO ₃	-2.16	-5.78 [40]
	-2.06	-5.51 [41]
	-1.75	-4.69 [16]
LuMnO ₃	-2.71	-7.55 [29]
	-3.89	-10.81 [17]

*Results calculated from crystal structure data in given references.

Figure Captions

Fig.1. (a) The crystal structure of hexagonal $REMnO_3$ showing the MnO_5 bipyramids and (b) the triangular lattice of Mn ions linked by oxygen atoms.

Fig.2. (a) X-ray powder diffraction patterns of $REMnO_3$ at various pressures ($T = 298$ K). From left panel to right panel are diffraction patterns of $YMnO_3$, $HoMnO_3$ and $LuMnO_3$, respectively. (b) Pressure dependent unit cell volumes (dots) and the first order Murnaghan fit (solid line) and (c) Compressibility of lattice parameters of a , c and V . The crosses are from the DFT calculations. Note the higher compressibility of the a-axis.

Fig.3. Pressure dependent fractional positions of Lu1 $2a$ ($0, 0, z$), Lu2 at $4b$ ($1/3, 2/3, z$) and Mn at $6c$ ($x, 0, z$) in (a) and the distance between Mn and Lu ions in (b).

Fig.4. The Mn K-edge x-ray absorption spectrum of hexagonal $LuMnO_3$ at ambient pressure and 16 GPa. Note that the overall shape of the spectra is unchanged. Only a shift of feature positions due to compression is observed.

Fig.5. Pressure dependent IR optical density spectrum of Hex- $REMnO_3$ at room temperature. (a) $YMnO_3$ IR absorption spectrum (Pressure: 0.00, 0.58, 1.17, 2.01, 3.02, 3.96, 4.98, 7.11, 7.97, 8.74, 9.35, 10.04, 10.99, 11.94, 12.98, 14.03, 15.08, 16.04, 17.11, 18.07, 19.40 GPa). (b) $HoMnO_3$ IR absorption spectrum (Pressure: 0.00, 0.58, 1.08, 2.01, 3.19, 4.13, 5.23, 5.91, 7.03, 8.14, 9.00, 10.29, 11.07, 12.56, 13.33, 14.03, 15.61, 16.40, 17.10, 18.25, 19.22, 20.46, 22.06 GPa). (c) $LuMnO_3$ IR absorption spectrum (Pressure: 0.00, 1.74, 2.95, 4.16, 5.30, 6.64, 7.99, 9.26, 10.88, 12.37, 14.04, 15.24, 17.31, 18.69, 20.65 GPa). (d) Ambient IR optical density spectra of Orthorhombic $DyMnO_3$.

Fig.6. Pressure dependent phonon frequencies of $YMnO_3$, $HoMnO_3$ and $LuMnO_3$.

Fig.7. Optical density spectrum of Hex- $LuMnO_3$ at RT, 373, 473, 573, 673K with the pressure at ~ 10 GPa, for each measurement.

Fig.8. Calculated E1 symmetry phonon modes for $LuMnO_3$ near ~ 310 cm^{-1} showing the displacement amplitudes and directions as vector lengths and directions (can be positive or negative), respectively. For these modes with large pressure dependence only the oxygen atoms have significant oscillation amplitudes with O ions moving in ab plane.

Fig.9. Calculated pressure dependent spontaneous polarization of Hex- $LuMnO_3$.

Fig.10. New peaks appear in x-ray diffraction pattern of Hex- $LuMnO_3$ (~ 22 GPa) and $YMnO_3$ (~ 24 GPa), (R means pressure release direction of measurement). The arrow indicates the new peak positions and corresponding peaks in an orthorhombic phase.

Fig.11. A qualitative Pressure-Temperature phase diagram for the $REMnO_3$ system (based on the $YMnO_3$).

Fig. 1. P. Gao *et al.*

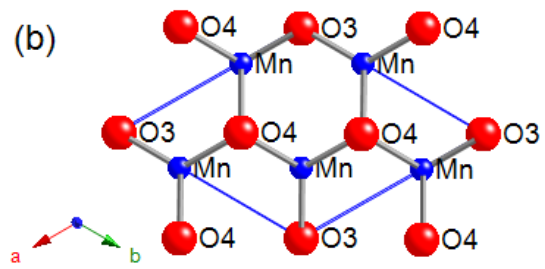
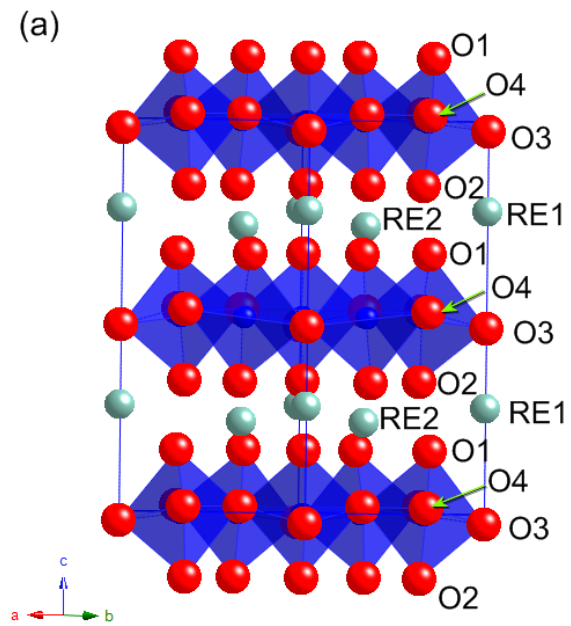


Fig. 2. P. Gao *et al.*

(a)

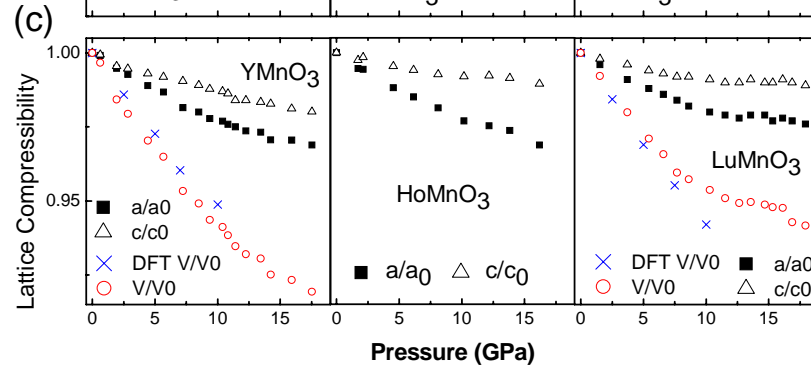
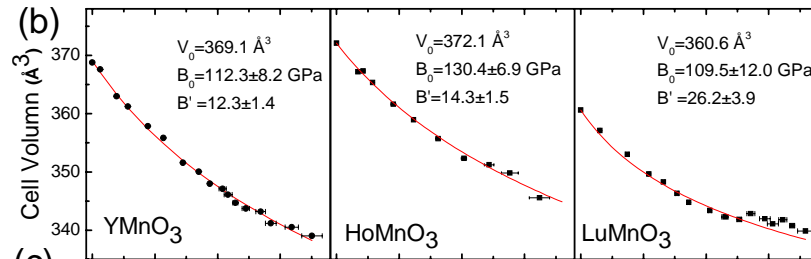
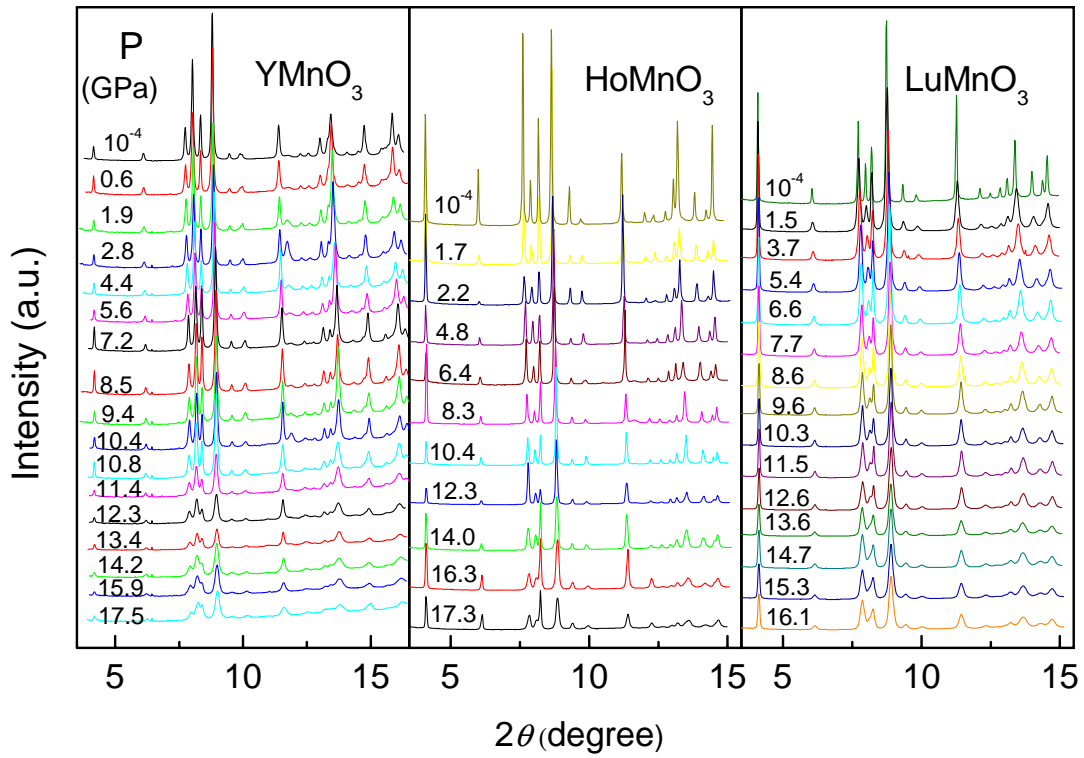


Fig. 3. P. Gao *et al.*

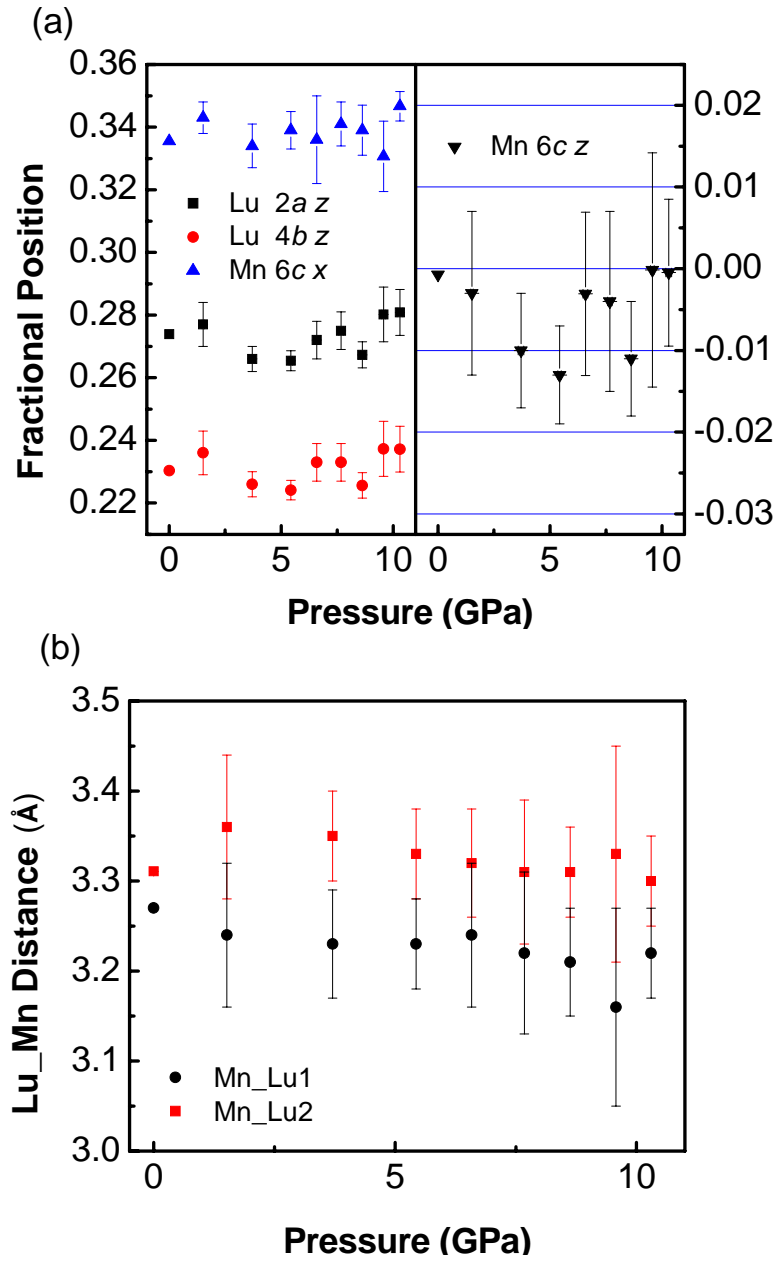


Fig. 4. P. Gao *et al.*

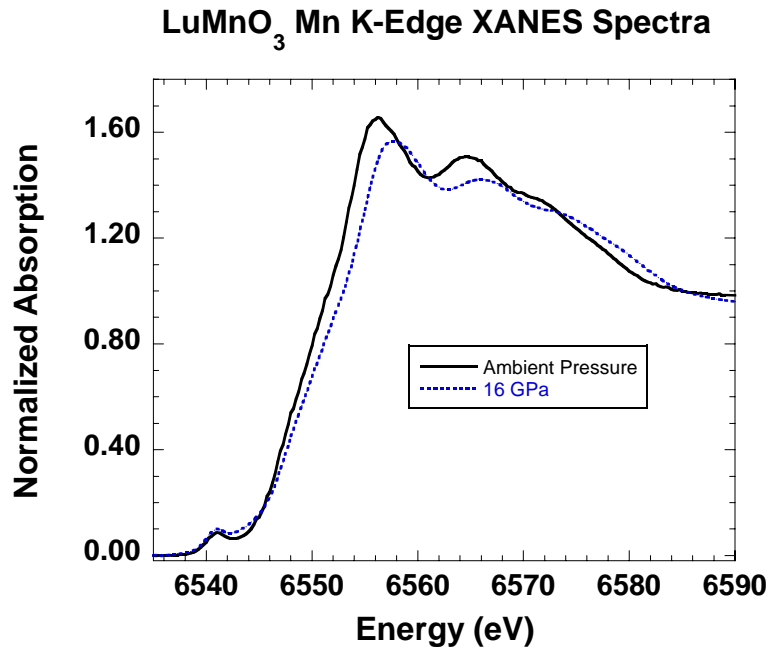


Fig. 5. P. Gao *et al.*

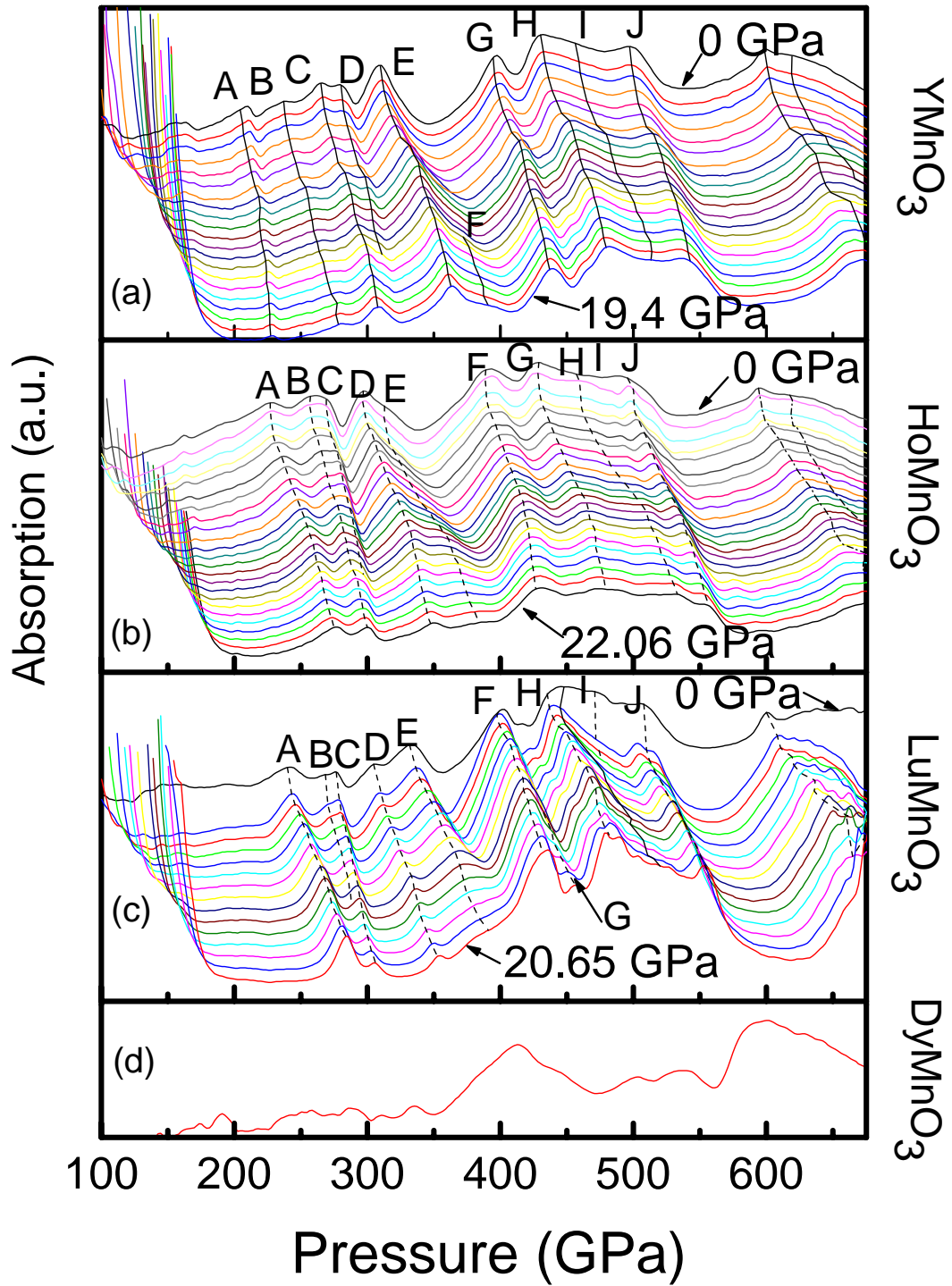


Fig. 6. P. Gao *et al.*

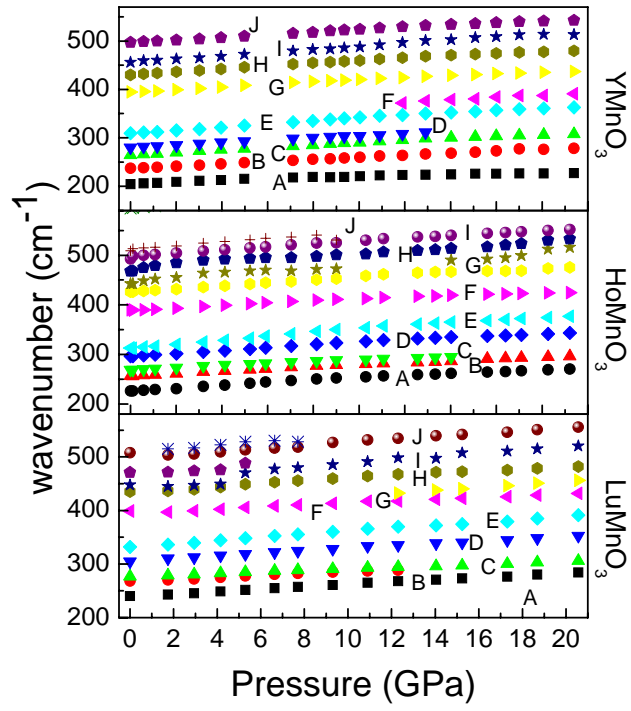


Fig.7. P. Gao *et al.*

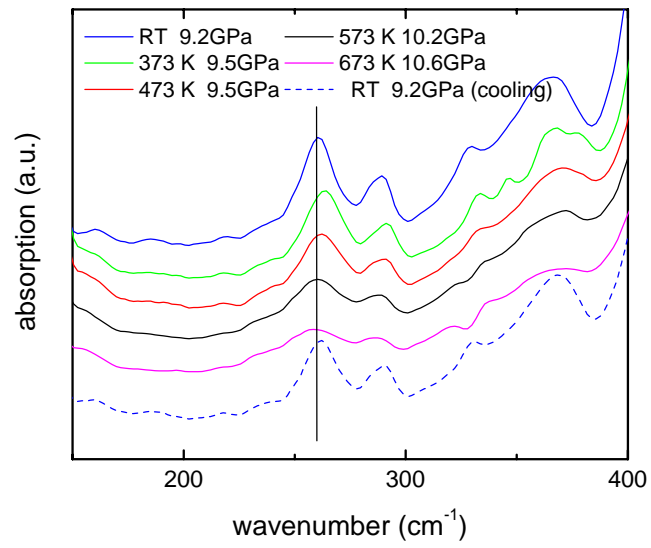


Fig. 8. P. Gao *et al.*

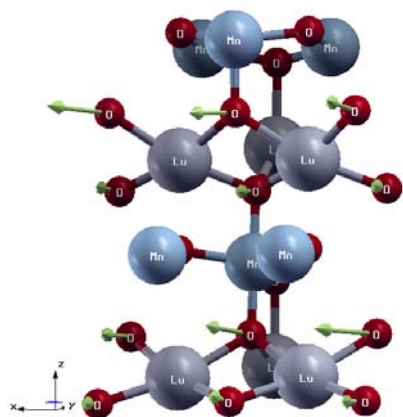
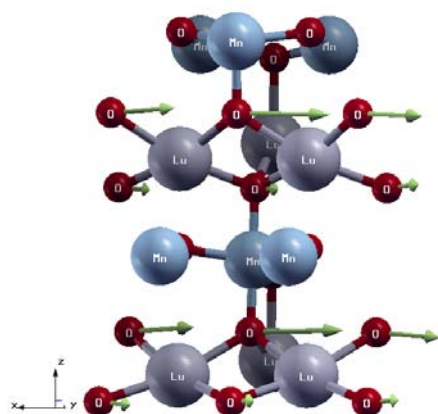


Fig. 9. P. Gao *et al.*

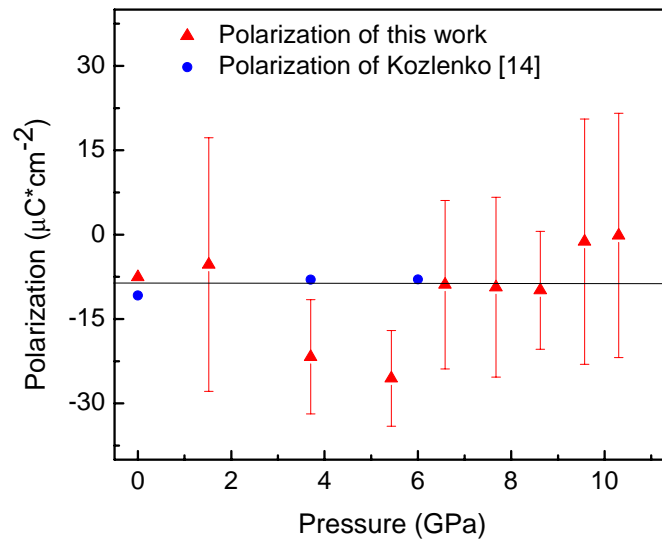


Fig. 10. P. Gao *et al.*

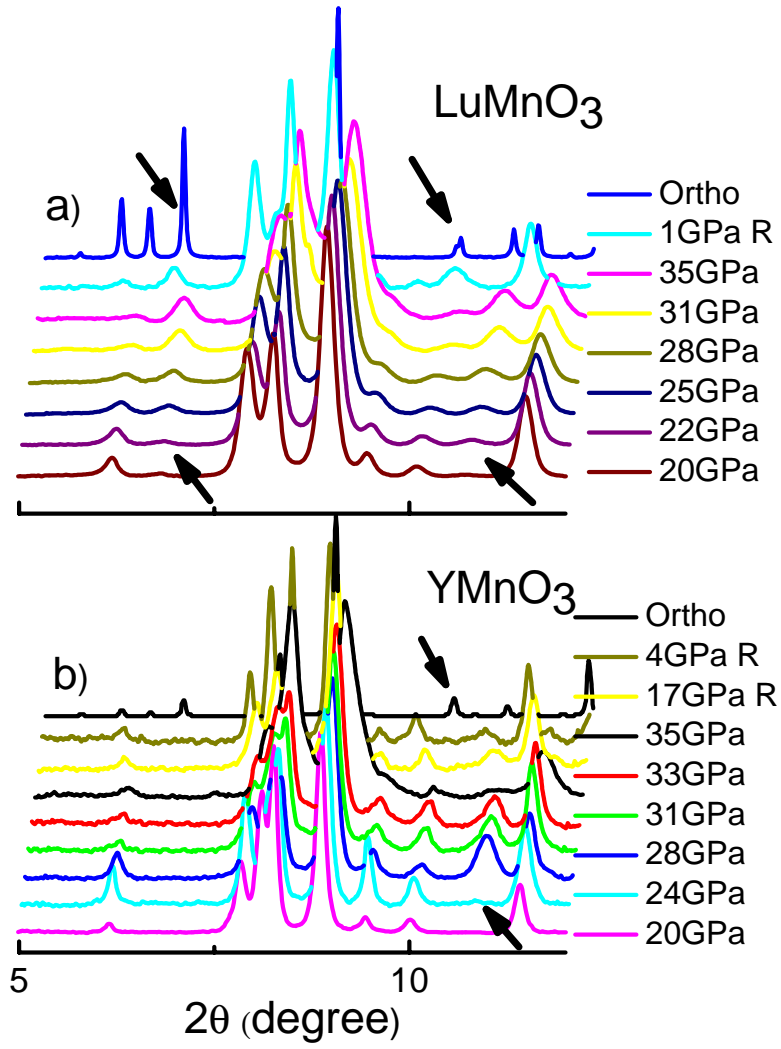
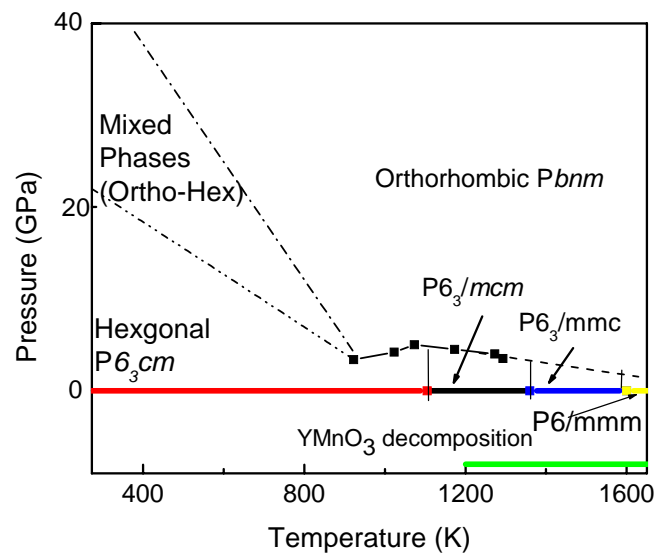


Fig. 11. P. Gao *et al.*



References

1. K. F. Wang, J.-M. Liu, and Z. F. Ren, *Adv. Phys.* **58**, 321 (2009).
2. A. B. Souchkov, J. R. Simpson, M. Quijada, H. Ishibashi, N. Hur, J. S. Ahn, S. W. Cheong, A. J. Millis, and H. D. Drew, *Phys. Rev. Lett.* **91**, 027203 (2003).
3. S. Abrahams, *Acta Crystallogr., Sect. B* **65**, 450 (2009).
4. O. P. Vajk, M. Kenzelmann, J. W. Lynn, S. B. Kim, and S. W. Cheong, *Phys. Rev. Lett.* **94**, 087601 (2005).
5. D. Fröhlich, S. Leute, V. V. Pavlov, and R. V. Pisarev, *Phys. Rev. Lett.* **81**, 3239 (1998).
6. B. Lorenz, Y. Q. Wang, Y. Y. Sun, and C. W. Chu, *Phys. Rev. B* **70**, 212412 (2004).
7. J. S. Zhou, J. B. Goodenough, J. M. Gallardo-Amores, E. Moran, M. A. Alario-Franco, and R. Caudillo, *Phys. Rev. B* **74**, 014422 (2006).
8. K. Uusi-Esko, J. Malm, N. Imamura, H. Yamauchi, and M. Karppinen, *Materials Chemistry and Physics* **112**, 1029 (2008).
9. H. Okamoto, N. Imamura, B. C. Hauback, M. Karppinen, H. Yamauchi, and H. Fjellvag, *Solid State Commun.* **146**, 152 (2008).
10. H. W. Brinks, H. Fjellvåg, and A. Kjekshus, *J. Solid State Chem.* **129**, 334 (1997).
11. P. A. Salvador, T.-D. Doan, B. Mercey, and B. Raveau, *Chem. Mater.* **10**, 2592 (1998).
12. C. Dubourdieu, G. Huot, I. Gelard, H. Roussel, O. I. Lebedev, and G. Van Tendeloo, *Philos. Mag. Lett.* **87**, 203 (2007).
13. I. Gelard, C. Dubourdieu, S. Pailhes, S. Petit, and C. Simon, *Appl. Phys. Lett.* **92**, 232506 (2008).
14. C. dela Cruz, F. Yen, B. Lorenz, Y. Q. Wang, Y. Y. Sun, M. M. Gospodinov, and C. W. Chu, *Phys. Rev. B* **71**, 060407 (2005).
15. M. Janoschek, B. Roessli, L. Keller, S. N. Gvasaliya, K. Conder, and E. Pomjakushina, *J. Phys.: Condens. Matter* **17**, L425 (2005).
16. D. Kozlenko, S. Kichanov, S. Lee, J. Park, V. Glazkov, and B. Savenko, *JETP Lett.* **82**, 193 (2005).
17. D. Kozlenko, S. Kichanov, S. Lee, J. Park, V. Glazkov, and B. Savenko, *JETP Lett.* **83**, 346 (2006).
18. D. Kozlenko, S. Kichanov, S. Lee, J. Park, V. Glazkov, and B. Savenko, *Crystallography Reports* **52**, 407 (2007).
19. D. P. Kozlenko, I. Mirebeau, J. G. Park, I. N. Goncharenko, S. Lee, J. Park, and B. N. Savenko, *Phys. Rev. B* **78**, 054401 (2008).
20. S. M. Feng, L. J. Wang, J. L. Zhu, F. Y. Li, R. C. Yu, C. Q. Jin, X. H. Wang, and L. T. Li, *J. Appl. Phys.* **103**, 026102 (2008).

21. A. P. Hammersley, S. O. Svensson, and A. Thompson, Nuclear Instruments and Methods in Physics Research Section A: Accelerators, Spectrometers, Detectors and Associated Equipment **346**, 312 (1994).
22. R. J. Angel, M. Bujak, J. Zhao, G. D. Gatta, and S. D. Jacobsen, Journal of Applied Crystallography **40**, 26 (2007).
23. F. M. Wang and R. Ingalls, Phys. Rev. B **57**, 5647 (1998).
24. W. A. BASSETT and E. HUANG, Science **238**, 780 (1987).
25. T. A. Tyson, T. Wu, K. H. Ahn, S. B. Kim, and S. W. Cheong, Phys. Rev. B **81**, 054101.
26. G. Kresse and D. Joubert, Phys. Rev. B **59**, 1758 (1999).
27. B. Toby, Journal of Applied Crystallography **34**, 210 (2001).
28. I. Loa, P. Adler, A. Grzechnik, K. Syassen, U. Schwarz, M. Hanfland, G. K. Rozenberg, P. Gorodetsky, and M. P. Pasternak, Physical Review Letters **87**, 125501 (2001).
29. B. B. Van Aken, A. Meetsma, and T. T. M. Palstra, Acta Crystallogr., Sect. E **57**, i101 (2001).
30. C. R. Natoli, edited by K. O. Hodgson, B. Hedman and J. E. Penner-Hahn (Springer-Verlag, New York, 1984), p. 38.
31. C. T. Wu, Y. Y. Hsu, B. N. Lin, and H. C. Ku, Physica B **329-333**, 709 (2003).
32. M. N. Iliev, H. G. Lee, V. N. Popov, M. V. Abrashev, A. Hamed, R. L. Meng, and C. W. Chu, Phys. Rev. B **56**, 2488 (1997).
33. A. Jayaraman, Reviews of Modern Physics **55**, 65 (1983).
34. T. Tohei, H. Moriwake, H. Murata, A. Kuwabara, R. Hashimoto, T. Yamamoto, and I. Tanaka, Phys. Rev. B **79**, 144125 (2009).
35. N. Fujimura, T. Ishida, T. Yoshimura, and T. Ito, Appl. Phys. Lett. **69**, 1011 (1996).
36. I. K. Jeong, N. Hur, and T. Proffen, Journal of Applied Crystallography **40**, 730 (2007).
37. M. Chen, B. Hallstedt, and L. J. Gauckler, J. Alloys Compd. **393**, 114 (2005).
38. B. B. Van Aken, Ph. D. dissertation., University of Groningen, 2001.
39. V. E. Wood, A. E. Austin, E. W. Collings, and K. C. Brog, J. Phys. Chem. Solids **34**, 859 (1973).
40. G. nert, M. Pollet, S. Marinel, G. R. Blake, A. Meetsma, and T. T. M. Palstra, J. Phys.: Condens. Matter **19**, 466212 (2007).
41. B. B. Van Aken, A. Meelsma, and T. T. M. Palstra, "Acta Crystallogr., Sect. C: Cryst. Struct. Commun. " **57**, 230 (2001).